Composites Science and Technology 72 (2012) 2016–2023

Contents lists available at SciVerse ScienceDirect

Composites Science and Technology

journal homepage: www.elsevier.com/locate/compscitech

Measurement of fibre waviness in industrial composite components

M.P.F. Sutcliffe [a,*], S.L. Lemanski [a], A.E. Scott [b]

[a] Cambridge University Engineering Department, Trumpington Street, Cambridge CB2 1PZ, UK
[b] School of Engineering Science, University of Southampton, Southampton, Hampshire SO17 1BJ, UK

ARTICLE INFO

Article history:
Received 9 May 2012
Received in revised form 30 July 2012
Accepted 1 September 2012
Available online 11 September 2012

Keywords:
A. Carbon fibres
B. Defects
D. Optical microscopy

ABSTRACT

Fibre orientation is measured from polished sections of the unidirectional plies of two industrial CFRP components made by resin transfer moulding (RTM) or prepreg/vacuum consolidation. The image analysis technique described by Creighton et al. [Composites: Part A 2001; 32: 221–229] is used to determine the fibre orientation over typically 5 × 5 mm sections. The standard deviation in fibre orientation angle is in the range 0.6–1.8°, being smallest for in-plane waviness of the prepreg component. The length and width of the waviness region along and transverse to the fibres is characterised using autocorrelation. The length is in the range 1.1–4.4 mm, being significantly greater in the prepreg than in the RTM component. The width is in the range 0.37–1.30 mm and is broadly similar across the sample types. It is demonstrated that the image analysis method can also be applied to X-ray images, giving good agreement with results from the polished prepreg samples.

1. Introduction

Compressive strength is an important property of fibre reinforced polymer matrix composites, but it is difficult to control and predict. There are various competing mechanisms of compressive failure, as reviewed by several authors, e.g. [1], but for standard engineering composites the governing failure mechanism is generally agreed to be plastic microbuckling. Argon [2], observing that fibre composites have regions of fibre misalignment, derived a simple expression for the compressive strength σ_c of unnotched material as $\sigma_c = k/\bar{\phi}$ where k is the in-plane shear yield stress of the composite and $\bar{\phi}$ is the initial misalignment angle of the uniformly misaligned fibres. This formula illustrates the critical role that fibre misalignment plays in determining compressive strength of fibre composites.

The size of the region of fibre misalignment also affects the compressive strength. Fibre bending stiffness causes an increase in compressive strength for small defects, but is negligible once the wavelength is greater than around 200 times the fibre diameter [3]. Lemanski and Sutcliffe [4] have shown that the compressive strength is sensitive to the ratio of the width of the wavy region to the width of a plate of finite size. Hence the spatial distribution of fibre orientation is also important for understanding and modelling compressive strength of fibre composites.

A variety of techniques have been developed to measure fibre waviness. Yurgatis [5] described a sectioning method, using the elliptical cross section of fibres cut on an oblique plane, to estimate fibre orientation. An automated version of this method has been used to measure large numbers of fibres with misalignments greater than 40° [6]. This method has the advantage of being able to measure orientation in two planes simultaneously, but relies on accurate cross-sectional geometry. More recently X-ray computed tomography has been used to measure fibre orientation. Salaberger et al. [7] measured the orientation of glass fibres in a polypropylene matrix, showing that the quality of the results depends on the algorithms used to derive the fibre orientation. Requena et al. [8] use synchrotron micro-tomography to image carbon fibre reinforced metal and polymer matrix composites. A series of image analysis steps is used to track the trajectory of individual fibres. The method is effective at measuring the three-dimensional fibre orientation field, although limited by the resources needed for such imaging and the relatively small volumes that can be measured. Creighton et al. [9] proposed the multiple field image analysis (MFIA) method to analyse relatively low-resolution micrographs of planes sectioned parallel to the nominal fibre direction. The standard deviation in the misalignment angle of prepreg, in a preliminary study, was found to be 0.7° [10]. An alternative image analysis algorithm based on Fourier analysis was developed by Kratmann et al. [11] and found to give an accuracy for the mean fibre angle of better than 0.2°. The technique has been used to analyse prepreg and pultruded samples [12]. Changes in pultrusion details reduced the standard deviation in the fibre misalignment angle from 1.3° to 0.9°. While the above techniques provide methodologies to measure fibre waviness, the methods have only been systematically applied to pultruded samples or a limited range of laboratory pre-preg samples. Wang et al. [13] present measurements of tow-level misalignment in an industrial component. Their

* Corresponding author. Tel.: +44 1223 332996; fax: +44 1223 332662.
E-mail address: mpfs@eng.cam.ac.uk (M.P.F. Sutcliffe).

0266-3538
http://dx.doi.org/10.1016/j.compscitech.2012.09.001

measurements relate to a specific defect associated with a nearby ply drop and a lay-up defect in an adjacent ply, so is representative of defects rather than a normal part of the sample. The paucity of data for real components has hindered model development and our understanding of the role of fibre waviness in compressive strength in industrial structures.

While knowledge of spatial variations in fibre misalignment are critically important, there is a lack of systematic measurement of the size of misaligned regions. Kyriakides et al. [14] observed using an optical microscope that the wavelength of fibre misalignment in APC-2/AS4 composites ranged between 2.1 and 5.6 mm. Clarke et al. [15,16] applied confocal laser-scanning microscopy to measure fibre waviness in a glass fibre-reinforced epoxy. They found, in preliminary results, wavelengths in the fibre direction typically within the range of 0.5–4 mm. This range of wavelengths was in good agreement with that observed by Wisnom [17] for carbon fibre composites. Potter et al. [18] observed a regular and systematic waviness in carbon fibre prepreg with a mean misalignment angle of 3.8° and a mean wavelength of 3 mm. Finally Liu et al. [10] found from spectral analysis that wavelengths of the order of a few 100 μm were predominant in CFRP material made from prepreg.

The theoretical work described above demonstrates the importance of both the angle and the spatial variation of fibre misalignment for compressive strength of long fibre composites. While there have been a number of studies measuring the misalignment angle of laboratory samples, relatively little research has characterised the spatial variation of fibre misalignment. Moreover the measurements have been almost entirely for well controlled laboratory samples which may not be typical of actual components. This study adopts the MFIA method for measurement of fibre orientation, with relatively minor extensions to increase efficiency. The method is used in two novel ways; as applied to industrial components and as a means to characterise both the misalignment angle and the spatial distribution of misalignment in fibre composite samples. Moreover we demonstrate that the analysis method, up to now applied to polished sections, can also be used with X-ray images.

2. Sample details

Two industrial components with standard lay-ups and manufacturing routes were provided by our collaborators. Both components had a predominantly 0° lay-up of unidirectional carbon fibres reinforced with epoxy, although other layers were present. One component was made from prepreg, consolidated under vacuum. The other was laid up as a dry preform and then resin transfer moulded (RTM). These are referred to as the 'prepreg' and 'RTM' components. Samples were taken from two representative locations on the two components. Both components had a slight curvature with in-plane dimensions significantly larger than the thickness, which was between 5 and 10 mm for the RTM component and between 10 and 30 mm for the prepreg component.

3. Imaging methodology

3.1. Orientation of sections

Section planes parallel and perpendicular to the surface of the component were used to measure in-plane and out-of-plane fibre waviness, as illustrated in Fig. 1, with corresponding in-plane and out-of-plane waviness misalignment angles ϕ. In all cases the zero direction for fibre orientation was taken as the mean fibre orientation angle in a section. The fibre angle varied as a function of position, and a prime is used to denote the standard deviation of the angle[1]. A characteristic length ℓ and width w for the waviness regions is also determined independently on the in-plane and out-of-plane sections, as illustrated schematically in Fig. 1.

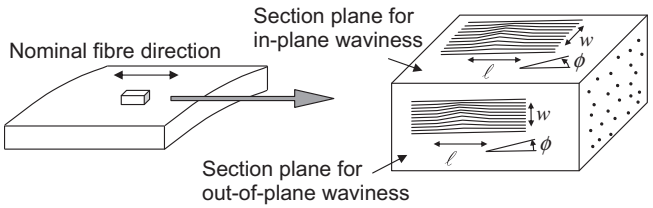

Fig. 1. Orientation of sections within samples.

3.2. Polished sections

Samples cut from the components were progressively polished, with a final polish using 3200 grit paper. Images were obtained using an Olympus BX51 optical microscope; the magnification was such that the pixel side length was 1.51 μm, giving adequate resolution to identify individual fibres. The section planes were nominally parallel to the fibres but there was inevitably some angular offset between these planes and the fibres, so that the fibres appeared as very elongated ellipses. Multiple images were taken using a motorised stage and stitched together using post-processing software [20], to give areas of typically around 5×5 mm. In total 16 analysis areas were measured, spanning the two specimens and both orientations. For the thicker prepreg sample the analysis area was predominantly 0° fibres. For the thinner RTM component the ply block thickness varied from a fraction of a millimetre to several millimetres, so that the regions of 0° material in the out-of-plane sections of this part necessarily covered a smaller area.

3.3. X-ray imaging

Micro-CT X-ray imaging was undertaken using a 225 kV Nikon/Metris HMX on a sample cut from the prepreg component. The imaging volume, obtained by concatenating images, was $4 \times 7 \times 12$ mm^3, with the longest dimension running along the fibre direction. A beam energy of 65 kV and current of 770 μA was used with a 2 s exposure. Two-dimensional radiographs were recorded at 2544 angular positions over 360° of rotation via a 2×2 k flat panel detector to give a voxel side length of 6.4 μm.

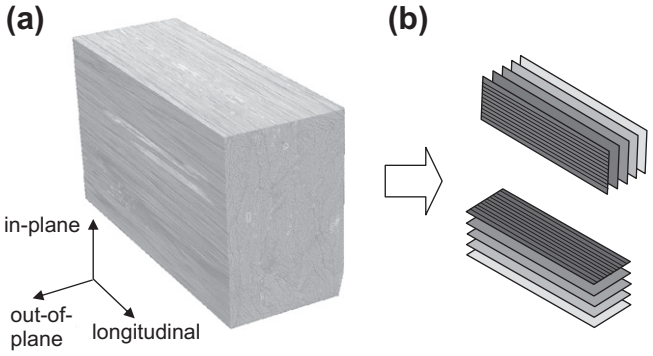

Fig. 2. X-ray data for prepreg specimen; (a) 3D data and (b) extraction of perpendicular slices.

[1] Although non-classical formulae should strictly be used to analyse the mean and standard deviation of angles [19], with the rather small range of angles in this study the classical formulae will give an error which is significantly less than the uncertainty in the measurements themselves.

Section planes in and out of the plane of the component were extracted from the 3D data at 100 μm intervals, as shown in Fig. 2.

4. Image analysis methodology

This section presents details of the method used to calculate fibre orientation and derive characteristic dimensions for the waviness features. A discussion of errors and sensitivity to analysis parameters is given in Section 4.3.

4.1. Estimate of fibre orientation angles

The MFIA method [9] is used to extract the fibre orientation from images of the polished and X-ray samples. There are many methods available for identification of orientation features, for example an FFT approach [11] or Hough transforms [21]. However the MFIA method was chosen as experience showed that this algorithm performs well for the given application. The method works by calculating the variation in correlation between features in the image and a 'trial' fibre, as a function of orientation angle of the trial fibre, averaged over a region of interest. The trial fibre orientation giving the minimum variation in the correlation function identifies the fibre angle within this region, as illustrated in Fig. 3. This bespoke algorithm is particularly effective because the fibre and matrix features defining the orientation are long thin bands of light and dark with a more-or-less uniform intensity. Three relatively minor changes were made to the original algorithm: (i) some optimisation of the code was undertaken to speed up the original algorithm, (ii) problems associated with alignment of fibres with the pixel direction were addressed and (iii) a more accurate method of determining the minimum in correlation was used. Previous developments of the MFIA method were limited by the calculation time [11], but the revised implementation was relatively rapid. The total CPU time required to analyse a typical micrograph was about 10 min on an Intel Core i7 2.8 GHz processor.

The circles shown in Fig. 4 give a typical variation of correlation function with trial angle. A quadratic function is fitted to the measured dependence of correlation function on orientation angle, through the data points close to the minimum. The minimum in this fit is used to determine the fibre orientation angle. There is a particular issue where the image edges are aligned with the fibre direction. Spurious peaks were seen in the correlation function when a large number of trial fibre orientations were used to determine the correlation function, as shown in Fig. 4. This perturbation,

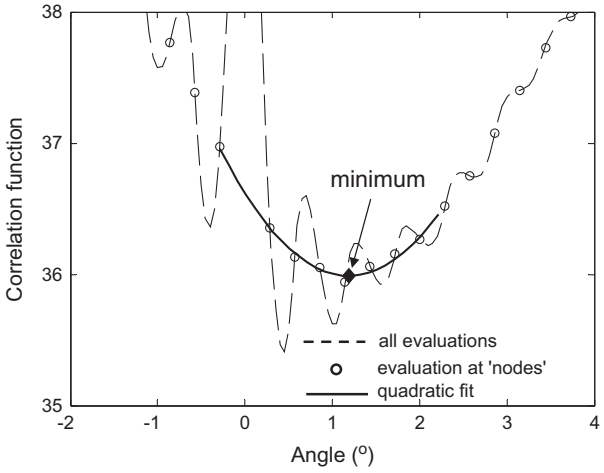

Fig. 4. Typical variation of correlation function with trial angle from a polished micrograph section. When a large number of angles are used spurious perturbations are introduced. Evaluation only at selected 'nodes' avoids these perturbations to give a smooth function which is fitted at the minimum by a quadratic.

which was also noted in [9], would cause an error in estimating the correct orientation angle. It was observed empirically that this error does not occur at angles equal to $\sin^{-1}(i/N)$, where i is an integer and N is the number of pixels in the averaging region in the fibre direction. Presumably the error is associated with the discrete nature of the pixel representation of the image, perhaps arising from interpolation of the image at an angle to the edges of the image. By using only angles equal to $\sin^{-1}(i/N)$ for the correlation evaluation, this error can be effectively eliminated, as shown by the circular markers at such 'nodes' plotted in Fig. 4. The effectiveness of this approach was checked by confirming that the resulting values of the correlation function averaged over many images did not contain spurious peaks. However the preferred approach is to ensure that fibres are not aligned along the pixel direction by appropriate alignment of the specimen with respect to the camera pixel orientation, so avoiding this problem.

Fig. 5 shows typical results for polished and X-ray images. The regions of interest over which the orientation is averaged are given by the inclined squares. An averaging area of side length 300 μm was used. The length of the 'trial fibre' was 40 μm for the polished samples and 64 μm for the X-ray image. Results are not sensitive to the choice of this length; these values were chosen as being

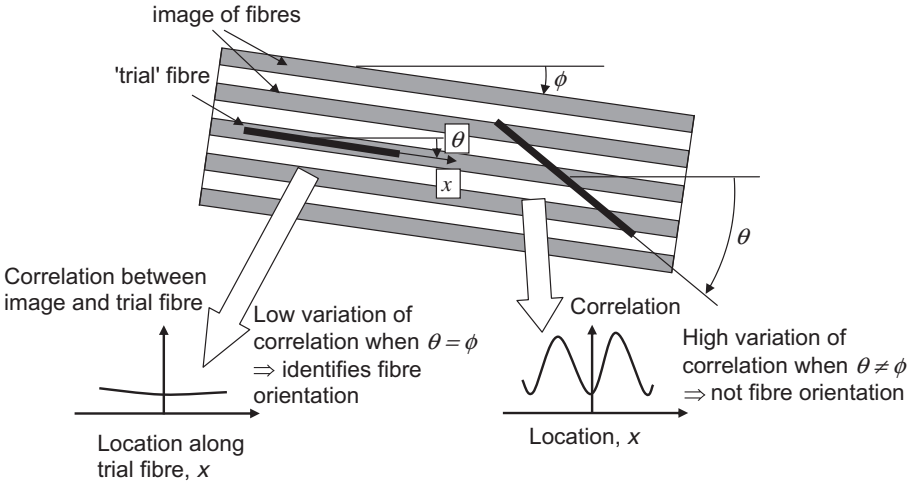

Fig. 3. MFIA method used to identify fibre angle. The trial fibre orientation θ giving the minimum variation in the correlation identifies the fibre angle ϕ.

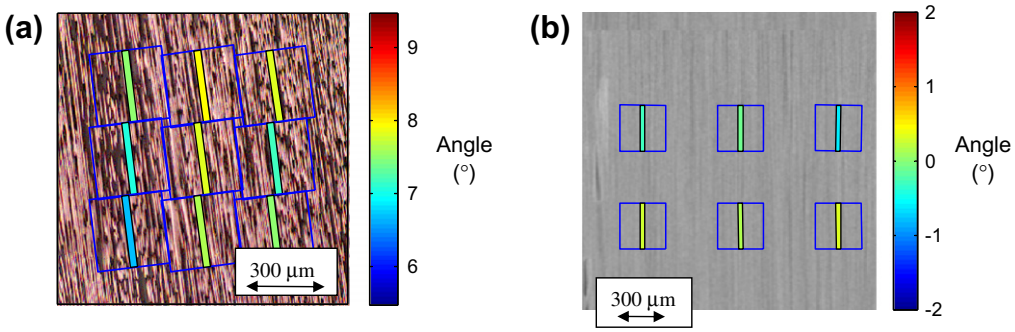

Fig. 5. Typical analyses of the fibre orientation angle: (a) polished micrograph sample and (b) X-ray image. The patch colour/grayscale value denotes the orientation angle in degrees, as per the scale bar. The superimposed squares show the extent of the averaging regions, which have side lengths of 300 μm.

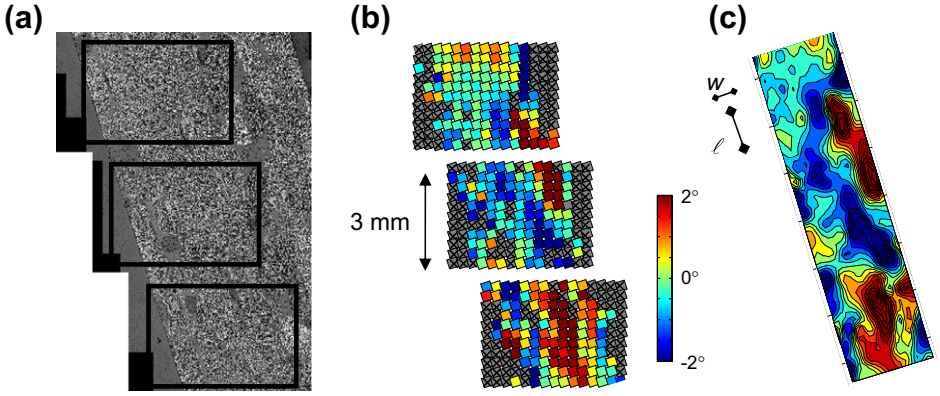

Fig. 6. Example of analysis of a polished micrograph section, (a) polished section, (b) fibre orientation map of 0° plies (contour scale bar gives the orientation, relative to the mean value, in degrees) and (c) interpolated gridded data, including correlation length and width of patch as estimated from the corresponding autocorrelation functions shown in Fig. 7. All images are to same scale, as per the scale bar. Grey patches containing crosses mark regions without a valid estimate of the orientation.

comparable to the length of the features observed in the images which ensured the robustness of the method. The slightly longer length for the X-ray image, corresponding to 10 pixels, was used on account of the larger pixel size for this data. The estimate of the fibre orientation is given by the colour/greyscale value of the patch within each box, as denoted by the scale bar. Estimates match well with a visual check. The image analysis algorithm was reasonably robust, even when the fibres were not so elongated because the sectioning plane was at a significant angle to the fibres or when the image not so sharp (e.g. because of polishing or focussing difficulties).

Fig. 6b shows the results of the analysis on the polished sample given in Fig. 6a. The orientation angle was evaluated at regions of interest of side-length 300 μm spaced 300 μm apart, to give around 300 measures of the fibre angle. In this case three sets of images have been stitched together, so evaluations have been avoided where images are joined. Regions in which a fibre orientation evaluation was not possible are indicated by grey patches and superimposed crosses. Many of these points correspond to areas outside the 0° plies, though there are some regions where the image quality was not good enough or where the fibre orientation was not well defined.

4.2. Characterisation of typical size of misaligned region

The method described above can extract the fibre orientation angle as a function of position. In this section we extend the work in [9] to estimate typical dimensions for the patches of misalignment. Previous work has used a spectral approach to estimating wavelengths [10]. Here we simplify the analysis to extract a single

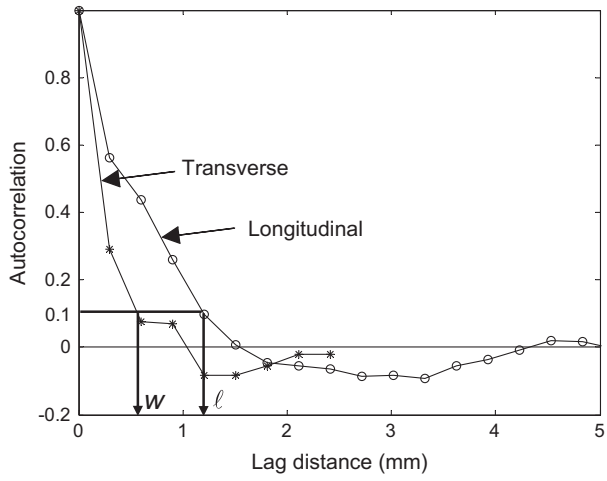

Fig. 7. Autocorrelation functions for data from Fig. 6 for a polished micrograph sample used to identify the correlation length and width of waviness regions.

measure for the characteristic length ℓ along the fibre direction and the width w transverse to the fibres of regions of misalignment. The analysis was undertaken by first selecting as large a rectangular region as possible which contains continuous 0° material from each section. The measured variation in misalignment angle data over the area was conditioned using the matlab *gridfit* algorithm [22], which generates a regular interpolating grid of values from a randomly spaced set of data and avoids difficulties with missed data points. Parameters were chosen to minimise smoothing of the dataset. Fig. 6c shows an example of the resulting interpolated

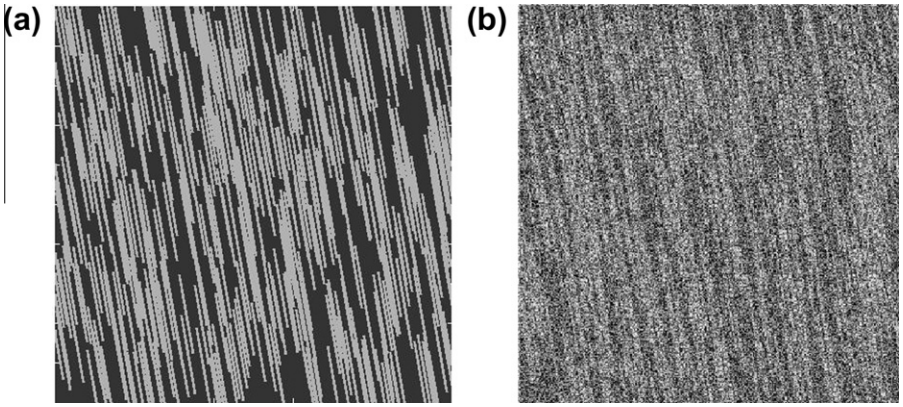

Fig. 8. Assessment of accuracy of fibre orientation, (a) typical artificial fibre pattern and (b) artificial pattern with noise which is beginning to degrade the accuracy. As these are artificial images there is no associated length scale.

data taken from the central region of the polished sample of Fig. 6a. A 2D autocorrelation function was then determined for the gridded data and used to find the autocorrelation functions along and transverse to the fibre direction. The autocorrelation function $R(x)$, scaled to equal one at zero lag x, is defined for a function $f(x)$ with mean μ and variance σ^2 as

$$R(x) = \frac{E[(f(x') - \mu)(f(x' + x) - \mu)]}{\sigma^2} \quad (1)$$

where E is the expected value operator. The correlation length is defined here as the lag distance x where the autocorrelation function equals 0.1, following standard practice in analysis of surface roughness length scales [23]. The autocorrelation function is used in a similar way to define a length scale in other fields, for example in turbulent flows [24]. Autocorrelation functions for the misalignment data given in Fig. 6 are plotted in Fig. 7. In this case the correlation length and width of waviness are estimated as 0.58 and 1.21 mm, respectively. These lengths are included in Fig. 6c, illustrating how the correlation length provides a reasonable approximation of the size of the waviness regions.

4.3. Discussion of potential errors and sensitivity to analysis parameters

There are three areas of error or uncertainty present in identification of fibre orientation: errors arising from poor definition of the orientation in the image, the accuracy of the algorithm itself and uncertainty over how to choose an appropriate area over which to average the fibre directions.

4.3.1. Poor definition of the orientation in the image

One of the advantages of the MFIA algorithm is that relatively low resolution microscope images can be used to extract a fibre orientation. Moreover it is not essential that the fibres are precisely sectioned along their length as long as a preferred orientation can be seen. However there comes a point at which the visual image no longer provides sufficient detail to detect a fibre direction. It is important with the automated approach to detect and exclude spurious orientation estimates arising, for example, where there are no 0° fibres, poorly polished regions or large non-fibre features (e.g. voids). On the other hand, where such 'missing data' occur, subsequent interpolation may miss real variations in misalignment near defects, so that it is important to minimise such exclusions. Hence the MFIA algorithm was modified to include three criteria which were used to validate an angle measurement: (i) the reduction in correlation function associated with alignment of the trial fibre and image features had to exceed a threshold value, typically 5% of the background value, (ii) a good fit was required between the calculated variation of correlation function with angle and a quadratic fit through the data near the minimum (typically the standard deviation in the difference between the data and the fit was less than 25% of the range of the correlation function), and (iii) the average intensity within the region had to fall within a specified range. A wide range was allowed for the last criterion,

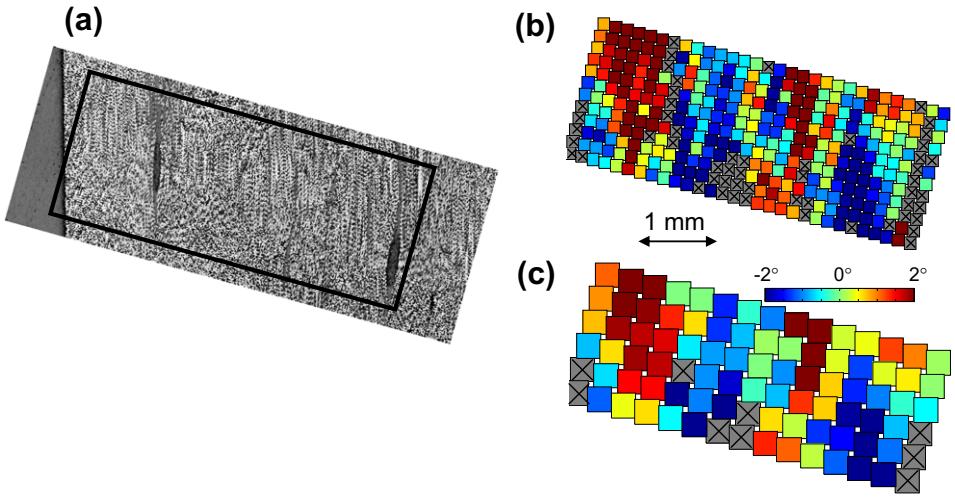

Fig. 9. Effect of analysis area on orientation angle for RTM sample. (a) polished micrograph section, (b) 150 μm averaging area side-length and (c) 300 μm side-length. The scale bar shown on the figure applies to all three images.

which was used to exclude in a simple way regions of the micrograph beyond the edge of the sample or plies which were not at a 0° orientation. Values of these validation parameters were tuned by comparison with visual examination for the particular type of image used. These criteria provided a robust and automated way of excluding regions which were obviously inappropriate, on closer inspection, as not covering regions with well defined fibre orientations, while not affecting the measurement for good parts of the image. Although the choice of these parameters was not critical, nevertheless it was important to select reasonable values to avoid spurious measurements. Alternative screening of appropriate parts of the sample, for example using manual segmentation, could have been used, although this would have been more cumbersome.

4.3.2. Accuracy of the algorithm

Visual spot-checks were made on the data to verify that the detected orientation matched a reasonable 'by eye' estimate. To assess the accuracy in an objective way, artificial fibre patterns were created with thin elliptical shapes all orientated at 10° but with random centre locations. Ten realisations were constructed, see Fig. 8a for an example. Using the standard algorithm with a relatively course interval between angle steps of 1°, the estimated angle differed from the nominal value of 10° by at most 0.13° in any of the 10 realisations. Introducing noise into the signal causes a significant reduction in accuracy only when the image itself is seriously degraded. For example the accuracy is still better than 0.17° for the image of Fig. 8b, which has random noise introduced at every pixel, with the level of noise uniformly distributed in the range ±194% of the difference between light and dark intensity levels. With this level of noise the measures for determining whether the angle estimate is valid are near the values used to reject estimates.

4.3.3. Choosing the averaging area

To guide the choice of averaging area, it is noted that fibre waviness patches of size smaller than about 100 times the fibre diameter d are significantly strengthened by fibre bending and so not critical to the strength. For the samples measured in this work, very local perturbations in fibre waviness appears to be relatively minor, so that it is appropriate to average over an area of side-length 150–600 μm, corresponding to 25–100d. The choice of averaging area is then dictated by the minimum size that gives an accurate estimate. Fig. 9 compares calculations of fibre orientation angle with averaging area side-lengths of 150 and 300 μm. The overall pattern of orientation is similar for the two analyses, but there seems to be some local variations for the smaller averaging area which may be unreliable. Moreover there are more data-points rejected as unreliable for the smaller sampling distance, as it becomes more difficult to extract the orientation over a small area. The standard deviation in the fibre orientation ℓ, taking the mean of three prepreg out-of-plane samples, equals 0.85°, 0.70° and 0.56° for averaging area side-lengths of 150, 300 and 600 μm, respectively. There is a significant decrease in ϕ' with increasing averaging area, as minor changes within the sample area are averaged out. There is a similar sensitivity of correlation length and width to sample area size. For example the correlation length ℓ, taking the mean of three prepreg out-of-plane samples, equals 1.22, 1.57 and 1.96 mm for averaging area side-lengths of 150, 300 and 600 μm, respectively. To give a compromise of reliability while maintaining adequate spatial sensitivity a side-length of 300 μm is chosen in the analysis.

5. Results

5.1. Polished sections

Fig. 10a and b shows typical normalised histograms of fibre orientation angles on out-of-plane sections, relative to the mean orientation, for prepreg and RTM samples. There is an approximately normal distribution of angles which can be characterised by the standard deviation ϕ' in the fibre orientation angle. Fig. 11a plots ϕ' for the different samples, grouped by section orientation and

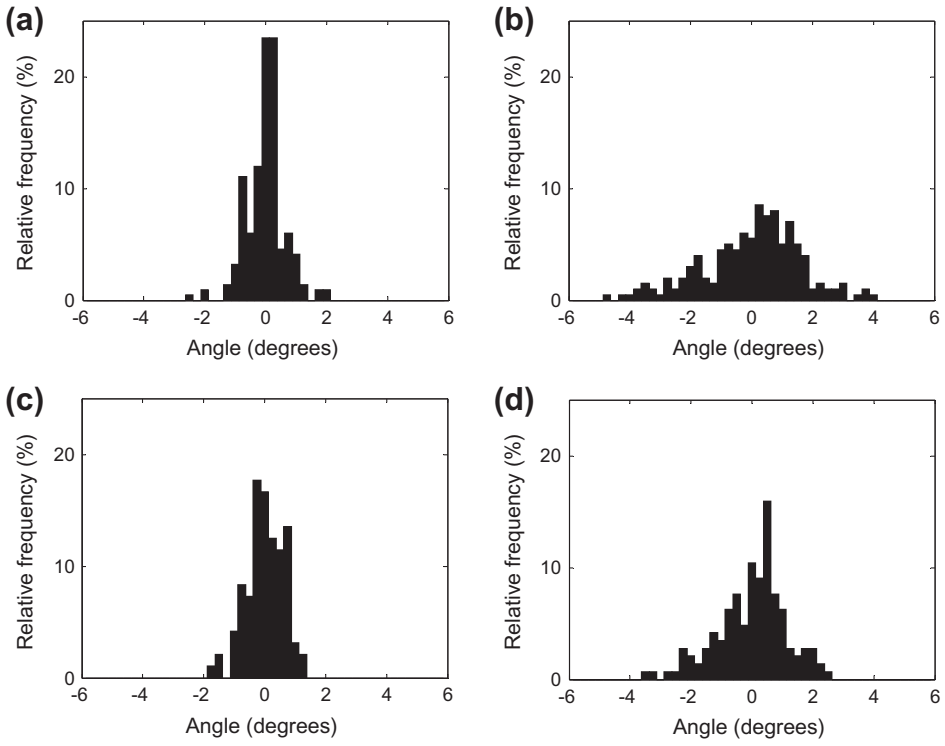

Fig. 10. Normalised histogram of fibre orientation angles, relative to the mean orientation, for: (a) polished micrographs of out-of-plane prepreg, (b) polished micrographs of out-of-plane RTM, (c) X-ray out-of-plane prepreg and (d) X-ray in-plane prepreg.

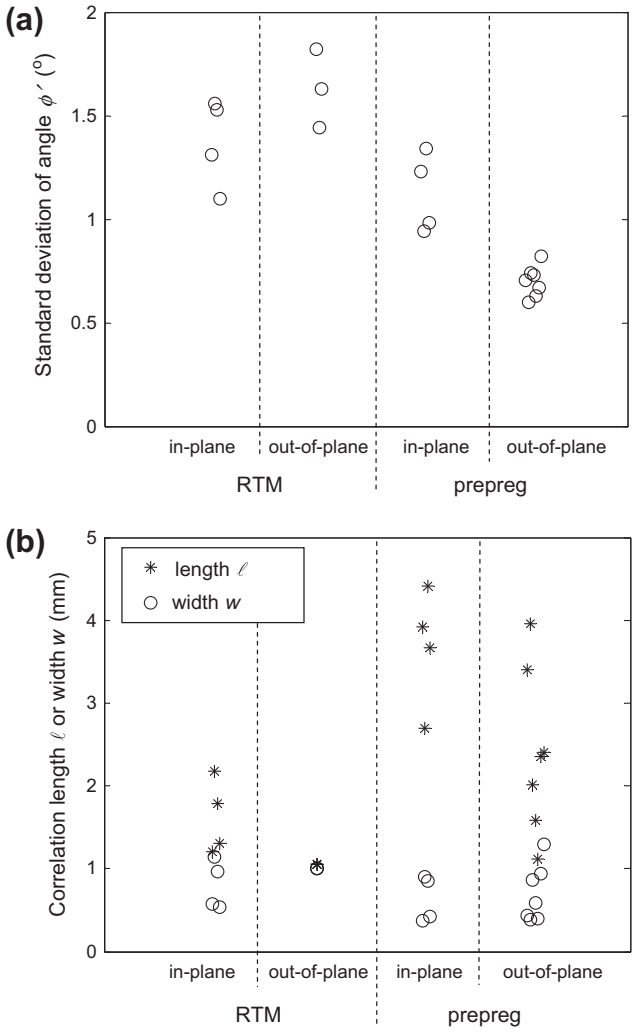

Fig. 11. Polished micrograph sample measurements: (a) standard deviation in fibre orientation and (b) correlation length scales.

component. Values are in the range 0.6–1.8°, i.e. similar to waviness data reported previously for carbon fibre composites [5,9,10,12]. The mean values of the angle standard deviations ϕ' for the prepreg component are 1.12° and 0.70°, for in-plane and out-of-plane sections, respectively. The corresponding values for the RTM in-plane and out-of-plane sections are 1.37° and 1.63°, respectively. The fibre mis-orientation angles for out-of-plane waviness of the prepreg component are significantly smaller than for the other sample measurements (significance at the 1% level confirmed using a Student's *t*-test). This probably reflects both differences in the fabric geometry and factors associated with the consolidation process.

Fig. 11b plots corresponding values of the correlation length ℓ and width w of the different samples. There is significant scatter within a given category, part of which may be due to the fact that the areas used for characterisation are relatively small compared with these correlation lengths. The mean values of the correlation length ℓ for the prepreg component are 3.7 mm and 2.4 mm, for in-plane and out-of-plane sections, respectively. Values for the RTM in-plane and out-of-plane sections are 1.6 mm and 1.1 mm, though in the later case there is only one data point rather than a mean as ply blocks were too thin to make a reliable evaluation of ℓ and w in most of these cases. These lengths match reported values in the literature for the wavelengths of waviness in carbon fibre composites [10,14–17]. Regions of waviness are significantly longer in the prepreg as compared with the RTM component (significance at the 5% level was confirmed using a Student's *t*-test, but results were not significant at the 1% level). The nature of the manufacturing process is presumably affecting these length scales. The width w of the patches tends to be significantly smaller than the length (significance at the 1% level confirmed using a Student's *t*-test), ranging from 0.37 to 1.30 mm, being broadly similar across the sample types. The mean width, averaging over all sample types, is 0.73 mm.

5.2. X-ray images

Fig. 10c and d shows histograms of fibre orientations, relative to the mean, from X-ray images of the prepreg sample. Again fibre angles are approximately normally distributed. The standard deviations of fibre orientation are 1.21° and 0.75° for in-plane and out-of-plane misalignment, respectively. These estimates agree well with values of 1.12° and 0.70° (in-plane and out-of-plane, respectively) for the mean of the standard deviations from all the corresponding polished samples.

An advantage of X-ray imaging is that in and out-of-plane misalignment angles can be measured at the same location, c.f. the results of Requena et al. [8]. It might be expected that factors causing high misalignment in one plane would lead to high misalignment in another. However an insignificant Pearson's correlation coefficient of 0.29 was observed between the misalignment angles in the two fibre orientations at the same location. This lack of correlation suggests that little extra information would be gained for these samples by characterising the waviness in a 3D manner, rather than using 2D slices from the images. However such a 3D quantification might add useful additional information where the quality of the sample imaging was relatively poor.

6. Conclusions

The method described by Creighton et al. [9] to measure fibre misalignment in composite materials has been improved and applied to the unidirectional ply blocks of carbon fibre in two industrial components. These were made either using resin transfer moulding or prepreg/vacuum consolidation. Measurement of waviness in the plane of the component and out-of-plane were undertaken by appropriate sectioning, either of polished samples or micro-CT X-ray images. Values for the standard deviation in fibre orientation angle were in the range 0.6–1.8°. The fibre alignment varied significantly less for in-plane waviness of the prepreg component, compared with the other sample measurements. The measurement technique of [9] has been extended using an autocorrelation function approach to characterise the length and width of the waviness region along and transverse to the fibres. The length of the waviness patch is in the range 1.1–4.4 mm, being significantly greater for the prepreg than the RTM component. The width of the patches tend to be significantly smaller than the length, ranging from 0.37 to 1.30 mm, being broadly similar across the sample types. Measurements of waviness from the X-ray images were in good agreement with the data from the polished sections, confirming the effectiveness of the fibre orientation measurement technique with X-ray images. The methods presented in this paper to characterise the spatial distribution of fibre orientation could equally be applied to other measurement techniques, either from polished micrographs [11] or X-ray imaging [7,8].

Acknowledgements

The authors acknowledge the support of EPSRC (reference EP/G012938/1) and MOD/DSTL, and thank colleagues at the Universities

of Cambridge and Bristol and at the industrial collaborators for their help, particularly with supply of the samples.

References

[1] Fleck NA. Compressive failure of fibre composites. Adv Appl Mech 1997;33:43–119.
[2] Argon AS. Fracture of composites, Treatise Mat Sci & Tech, vol. 1. New York: Academic Press; 1972.
[3] Shu JY, Fleck NA. Microbuckle initiation in fibre composites under multiaxial loading. Proc Roy Soc 1997;A453:2063–83.
[4] Lemanski SL, Sutcliffe MPF. Compressive failure of finite size unidirectional composite laminates with a region of fibre waviness. Composites Part A 2012;43:435–44.
[5] Yurgartis SW. Measurement of small angle fiber misalignments in continuous fiber composites. Compos Sci Technol 1987;30:279–93.
[6] Barwick SC, Papathanasiou TD. Identification of sample preparation defects in automated topological characterization of composite materials. J Reinf Plast Compos 2003;22:655–69.
[7] Salaberger D, Kannappan KA, Kastner J, Reussner J, Auinger T. Evaluation of computed tomography data from fibre reinforced polymers to determine fibre length distribution. Int Polym Process 2011;26:283–91.
[8] Requena G, Fiedler G, Seiser B, Degischer P, Di Michiel M, Buslaps T. 3D-quantification of the distribution of continuous fibres in unidirectionally reinforced composites. Composites: Part A 2009;40:152–63.
[9] Creighton CJ, Sutcliffe MPF, Clyne TW. A multiple field image analysis procedure for characterisation of fibre alignment in composites. Composites: Part A 2001;32:221–9.
[10] Liu D, Fleck NA, Sutcliffe MPF. Compressive strength of fibre composites with random fibre waviness. J Mech Phys Solids 2004;52:1481–505.
[11] Kratmann KK, Sutcliffe MPF, Lilleheden LT, Pyrz R, Thomsen OT. A novel image analysis procedure for measuring fibre misalignment in unidirectional fibre composites. Compos Sci Technol 2009;69:228–38.
[12] Kratmann KK, Thomsen OT. Experimental characterisation of parameters controlling the compressive failure of pultruded unidirectional carbon fibre composites. Appl Mech Mater 2010;24–25:15–22.
[13] Wang J, Potter KD, Hazra K, Wisnom MR. Experimental fabrication and characterization of out-of-plane fibre waviness in continuous fibre-reinforced composites. J Compos Mater 2012;46:2041–53.
[14] Kyriakides S, Arseculeratne R, Perry EJ, Liechti KM. On the compressive failure of fibre reinforced composites. Int J Solids Struct 1995;32:689–738.
[15] Clarke AR, Archenhold G, Davidson NC. A novel technique for determining 3D spatial distribution of glass fibres in polymer composites. Compos Sci Technol 1995;55:75–91.
[16] Clarke AR, Archenhold G, Davidson NC, Fleck NA. Determining the power spectral density of the waviness of unidirectional glass fibres in polymer composites. Appl Compos Mater 1995;2:233–43.
[17] Wisnom MR. The effect of fibre waviness on the relationship between compressive strength of unidirectional composites. J Compos Mater 1994;28:66–76.
[18] Potter KD, Langer C, Hodgkiss B, Lamb S. Sources of variability in uncured aerospace grade unidirectional carbon fibre epoxy preimpregnate. Composites: Part A 2007;38:905–16.
[19] Mardia KV, Jupp P. Directional statistics. 2nd ed. John Wiley and Sons Ltd.; 2000.
[20] d'Angelo P. Hugin-2010.2.0. 2010: <http://hugin.sourceforge.net>. [accessed 29.06.2012].
[21] Illingworth J, Kittler J. A survey of the Hough transform. Comp Vision Graph Image Process 1988;44:87–116.
[22] D'Errico J. 2010. Surface fitting using gridfit. 2010: <http://www.mathworks.de/matlabcentral/fileexchange/8998>. [accessed 29.06.2012].
[23] Williams JA. Engineering tribology. Cambridge University Press; 2005.
[24] Tennekes H, Lumley JL. A first course in turbulence. MIT Press; 1972.